PHYSICAL REVIEW D **83,** 014010 (2011)

Origin of light 0^+ scalar resonances

Zhi-Yong Zhou* and Zhiguang Xiao†

Department of Physics, Southeast University, Nanjing 211189, People's Republic of China, and Institute for Particle Physics Phenomenology, Durham University, Durham DH1 3LE, United Kingdom
School of Physics and Astronomy, University of Southampton Highfield, Southampton, SO17 1BJ, United Kingdom, and Interdisciplinary Center for Theoretical Study, University of Science and Technology of China, Hefei, Anhui 230026, China

(Received 2 July 2010; published 18 January 2011)

We demonstrate how most of the light $J^P = 0^+$ spectrum below 2.0 GeV and their decays can be consistently described by the unitarized quark model incorporating the chiral constraints of Adler zeros and taking $SU(3)$ breaking effects into account. These resonances appear as poles in the complex s plane in a unified picture as $q\bar{q}$ states strongly dressed by hadron loops. Through the large N_c analysis, these resonances are found to naturally separate into two kinds: σ, κ, $f_0(980)$, $a_0(980)$ are dynamically generated and run away from the real axis as N_c increases, while the others move towards the $q\bar{q}$ seeds. In this picture, the line shape of $a_0(980)$ is produced by a broad pole below the $K\bar{K}$ threshold, and exhibits characteristics similar to the σ and κ.

DOI: 10.1103/PhysRevD.83.014010 PACS numbers: 12.39.Ki, 11.55.Bq, 13.75.Lb, 14.40.Be

I. INTRODUCTION

The enigmatic spectrum of light $J^P = 0^+$ scalar resonances are of great interest for its importance in understanding chiral symmetry breaking and confinement in QCD. Despite many theoretical efforts, the current understanding of the microscopic structures of these resonances is in a well-known unclear situation as summarized in Particle Data Group (PDG) [1]: $q\bar{q}$ models [2], the unitarized meson model [3], a tetraquark model with and without $q\bar{q}$ mixing [4,5], the Jülich meson exchange model [6], the unitarized σ model [7], glueball [8] or using the inverse amplitude method (IAM) [9], NJL model [10] and lattice simulations [11], and so on. Most of these studies focus on the lowest putative nonet or explain the lighter and heavier resonances in different ways. In the present paper, we show that all the light scalar spectrum below 2.0 GeV except a glueball candidate can be described (or even predicted) using just seven parameters in a unified and consistent picture, that is, $q\bar{q}$ seeds strongly dressed by hadron loops. The picture brings more insights on the origin of the resonances, which are generated as the poles of the S matrix and have no one-to-one correspondence with the nonet in the Lagrangian. At the weak coupling limit as N_c increases, σ, κ, $a_0(980)$, and $f_0(980)$ move away from the real axis on the complex energy plane, whereas all the other heavier $J^P = 0^+$ resonances move to the bare seeds. This reveals the differences between the lighter mesons and heavier states.

We use the unitarized quark model (UQM) [2] proposed by Törnqvist, which played a pioneering role in the resurrection of the σ meson. The merit of this model is that it naturally respects the unitarity of the S matrix but also incorporates some dynamics at the same time. Besides, the Adler zeros [12], as the constraints from chiral symmetry, can also be easily implemented. Nevertheless, the κ resonance was not found in his explicit analysis of experimental data, and those resonances with higher masses than 1.5 GeV are also not covered. In the present paper, however, by incorporating the $SU(3)$ breaking effects in the coupling constants and analyzing the poles on the complex plane, we show that the κ resonance can really be found in this picture. Moreover, most resonances in $I = 0$, $I = 1/2$, and $I = 1$ channels can find their corresponding poles on the complex plane.

The paper is organized as follows: In Sec. II, we briefly introduce the basic scheme of UQM and the three nontrivial improvements we make to this model. Our numerical results are elaborately discussed in Sec. III. Section IV is devoted to a further study on the characteristics of these resonances based on the large N_c technique. Section V summarizes our main results.

II. THE THEORETICAL SCHEME

A. Unitarized quark model

The unitarized quark model begins by assuming that there are $q\bar{q}$ bare bound states generated in QCD and they are coupled with the pseudoscalar mesons. The main idea is to take into account the hadron loop dressing effect in the propagators of the bare $q\bar{q}$ states [2,13]. The bare propagator of a $q\bar{q}$ bound state is

$$P = \frac{1}{m_0^2 - s}, \tag{1}$$

where m_0 is the bare mass. For example, m_0 is $2\hat{m}$ for $u\bar{u}$ or $d\bar{d}$, $\hat{m} + \Delta m$ for $u\bar{s}$, and $2\hat{m} + 2\Delta m$ for $s\bar{s}$ state, respectively. The vacuum polarization function, $\Pi(s)$, which

*zhouzhy@seu.edu.cn
†xiaozg@ustc.edu.cn

represents all the possible two pseudoscalar meson loops, will contribute to the full propagator as

$$P = \frac{1}{m_0^2 - s + \Pi(s)}. \tag{2}$$

As an analytic function with a right-hand cut, its real and imaginary parts are related by a dispersive integral

$$\mathrm{Re}\,\Pi(s) = \frac{1}{\pi}\mathcal{P}\int_{s_{\mathrm{th}}}^{\infty} dz\,\mathrm{Im}\Pi(z)/(z-s), \tag{3}$$

where

$$\mathrm{Im}\,\Pi(s) = -\sum_i G_i(s)^2 = -\sum_i g_i^2 \frac{k_i(s)}{\sqrt{s}} F_i(s)^2 \theta(s - s_{\mathrm{th},i}), \tag{4}$$

where the general coupling function $G_i(s)$ includes the coupling constants g_i's, the phase space factor $k_i(s)/\sqrt{s}$, and a Gaussian form factor $F_i(s) = \exp[-k_i^2(s)/2k_0^2]$. $k_i(s)$ is the ith channel c.m. momentum with $k_i(s) = \sqrt{\lambda(s, m_{A_i}^2, m_{B_i}^2)/4s}$ and the $\theta(s - s_{\mathrm{th},i})$ is a unit step function.

If there exists more than one bare state in the $i \to j$ channel, the partial-wave amplitude can be represented in a more general matrix form:

$$\begin{aligned} T_{ij} &= \sum_{\alpha,\beta} G_{i\alpha} P_{\alpha\beta} G_{j\beta}^*, \\ \{P^{-1}\}_{\alpha\beta}(s) &= (m_{0,\alpha}^2 - s)\delta_{\alpha\beta} + \Pi_{\alpha\beta}(s), \\ \mathrm{Im}\Pi_{\alpha\beta}(s) &= -\sum_i G_{i\alpha}(s) G_{\beta i}^*(s) \\ &= -\sum_i g_{\alpha i} g_{\beta i} \frac{k_i(s)}{\sqrt{s}} F_i^2(s)\theta(s - s_{\mathrm{th},i}), \end{aligned} \tag{5}$$

where $\mathrm{Re}\Pi_{\alpha\beta}$ is determined by a similar dispersion integral of $\mathrm{Im}\Pi_{\alpha\beta}$ as Eq. (3). The off-diagonal terms of $\Pi_{\alpha\beta}$ produce the mixing between different bare states coupled with the same intermediate states.

The Adler zeros are incorporated into the UQM model in a direct and easily operated phenomenological way [2]:

$$G_{\alpha i}(s) G_{\beta i}(s) \to \gamma_{\alpha i}\gamma_{\beta i}(s - z_{A,i}) F_i^2(s) \frac{k_i(s)}{\sqrt{s}} \theta(s - s_{\mathrm{th},i}), \tag{6}$$

where the $z_{A,i}$'s denote the Adler zeros, and $\gamma_{\beta i}$ are dimensionless coupling constants.

B. The Adler zeros in the chiral perturbation theory

Normally, the T matrix also contains left-hand cuts. Because the Adler zero is usually located nearer to the physical threshold than the left-hand cut, it is natural to expect that it plays a more important role than the left-hand cut in determining the scattering amplitudes along the right-hand cut. Since such zeros reflect the constraints of the chiral symmetry, in the $I = 0, 1/2$ channels, they are fixed in our study at the values obtained from the chiral perturbation theory (ChPT) [14] rather than left as free parameters. In the $I = 1$ channel, we also fix the Adler zero according to ChPT but there are some subtleties which will be addressed later. Being within the convergence radius of the chiral expansion, these Adler zeros should be reliably determined by ChPT and, hence, is a reasonable starting point for a phenomenological study.

After partial-wave expansion, one obtains the Adler zero of $I = 0$ $\pi\pi$ S wave at about $m_\pi^2/2$ at tree level, and the position is slightly shifted to $s \simeq 0.38 m_\pi^2$ by including the contribution up to two-loop $SU(2)$ ChPT [15]. Similarly, in the $K\pi$ scattering, the $SU(3)$ ChPT to $O(p^2)$ gives S-wave amplitude of $I = 1/2$ as

$$T_{I=1/2}^{l=0}(s) = \frac{-3(m_K^2 - m_\pi^2)^2 - 2(m_K^2 + m_\pi^2)s + 5s^2}{128\pi f_K f_\pi s}, \tag{7}$$

which has two zeros located at $\frac{1}{5}(m_K^2 + m_\pi^2 \pm 2\sqrt{4m_K^4 - 7m_K^2 m_\pi^2 + 4m_\pi^4})$ in the unphysical region. One is on the negative real axis inside the circular cut, and the other is on the positive axis between the circular cut and the $K\pi$ threshold. With the $O(p^4)$ contribution, the left zero on the negative axis moves to the complex s plane at about $s = 0.003 \pm 0.005i$ GeV^2 and the right one on the positive axis will also be slightly shifted (at about $s = 0.233$ GeV^2). As for the $\pi\eta$ scattering, at leading order $O(p^2)$, ChPT recovers the current-algebra result [16]:

$$T_{\pi\eta}^{(2)}(s, t, u) = \frac{m_\pi^2}{3f_\pi^2}, \tag{8}$$

which contains no zero on the real s axis after the partial-wave projection. Including the higher order contribution is not helpful to obtain a real-valued Adler zero. A pair of zeros, at about $0.078 \pm i0.178$ GeV^2, can be found when the $O(p^4)$ terms are taken into account using the low-energy constants from Ref. [17]. Since there is no accurate data of the $\pi\eta$ scattering, we could choose a zero point on the real axis to simulate them as mentioned later.

C. The scalar-pseudoscalar-pseudoscalar coupling

The coupling of pseudoscalar-pseudoscalar to the 0^+ states could be described by effective interaction terms in the Lagrangian: $\mathcal{L}_{SPP} = \alpha Tr[SPP] + \beta Tr[S]Tr[PP] + \gamma Tr[S]Tr[P]Tr[P]$. The first term has an $SU(3)$-symmetric quarkonium coupling as used in many phenomenological models. We also include the Okubo-Zweig-Iizuka violation terms in the last two terms in a general way. Moreover, the decay of the quarkonium into a pair of mesons $Q\bar{Q} \to M(Q\bar{q}_i)M(q_i\bar{Q})$ involves the creation of a $q_i\bar{q}_i$ pair from the vacuum. The ratio of the creation rates of $s\bar{s}$ and $u\bar{u}$ or $d\bar{d}$ from the vacuum is usually defined as $\rho = \langle 0|V|s\bar{s}\rangle/\langle 0|V|u\bar{u}\rangle$, representing

TABLE I. The effective scalar quarkonium coupling to pseudoscalar mesons up to a global constant.

I		Coupling coefficient
$0(n\bar{n})$	$\pi\pi$	$-\sqrt{3}\alpha - 2\sqrt{3}\beta$
	$K\bar{K}$	$-\rho\alpha - 4\beta$
	$\eta\eta$	$\cos\phi^2\alpha + 2\beta + 2(1 + \cos\phi^2 - \sqrt{2}\sin2\phi)\gamma$
	$\eta\eta'$	$\frac{\sin2\phi}{\sqrt{2}}\alpha + (4\cos2\phi + \sqrt{2}\sin2\phi)\gamma$
	$\eta'\eta'$	$\sin\phi^2\alpha + 2\beta + 2(1 + \sin\phi^2 + \sqrt{2}\sin2\phi)\gamma$
$0(s\bar{s})$	$\pi\pi$	$-\sqrt{6}\beta$
	$K\bar{K}$	$-\sqrt{2}\alpha - 2\sqrt{2}\beta$
	$\eta\eta$	$\sqrt{2}(\rho\sin\phi^2\alpha + \beta + (1 + \cos\phi^2 - \sqrt{2}\sin2\phi)\gamma)$
	$\eta\eta'$	$-\rho\sin2\phi\alpha + 2\sqrt{2}\cos2\phi\gamma + \sin2\phi\gamma$
	$\eta'\eta'$	$\sqrt{2}(\rho\cos\phi^2\alpha + \beta + (1 + \sin\phi^2 + \sqrt{2}\sin2\phi)\gamma)$
1	$\eta\pi$	$\sqrt{2}\cos\phi\alpha$
	$K\bar{K}$	$-\rho\alpha$
	$\eta'\pi$	$\sqrt{2}\sin\phi\alpha$
1/2	$K\pi$	$-\sqrt{3/2}\alpha$
	$K\eta$	$(\frac{\cos\phi}{\sqrt{2}} - \rho\sin\phi)\alpha$
	$K\eta'$	$(\frac{\sin\phi}{\sqrt{2}} + \rho\cos\phi)\alpha$

the breaking of $SU(3)$ symmetry [18]. $SU(3)$ breaking effects have proved to be important, so we allow for these in our version of the UQM. To be explicit about our description of the coupling of quarkonium to mesons, we express the scalar and pseudoscalar 3×3 flavor matrices in $q\bar{q}$ configurations as

$$S = \begin{pmatrix} \frac{1}{\sqrt{2}}a^0 + \frac{1}{\sqrt{2}}f_n & a^+ & \kappa^+ \\ a^- & \frac{-1}{\sqrt{2}}a^0 + \frac{1}{\sqrt{2}}f_n & \kappa^0 \\ \kappa^- & \bar{\kappa}^0 & f_s \end{pmatrix}, \quad (9)$$

$$P = \begin{pmatrix} \frac{\sqrt{3}\pi^0 + \eta_8}{\sqrt{6}} & \pi^+ & K^+ \\ \pi^- & \frac{-\sqrt{3}\pi^0 + \eta_8}{\sqrt{6}} & K^0 \\ K^- & \bar{K}^0 & -\sqrt{\frac{2}{3}}\eta_8 \end{pmatrix} + \frac{1}{\sqrt{3}}\eta_1, \quad (10)$$

where $f_n = n\bar{n} \equiv (u\bar{u} + d\bar{d})/\sqrt{2}$ and $f_s = s\bar{s}$. The physical states, η and η', are conventionally defined as $\eta = \cos\phi|n\bar{n}\rangle - \sin\phi|s\bar{s}\rangle$, $\eta' = \sin\phi|n\bar{n}\rangle + \cos\phi|s\bar{s}\rangle$, with $\phi = \tan^{-1}\sqrt{2} + \theta_P$, where $\theta_P = -11.5°$ being the pseudoscalar octet-singlet mixing angle [1]. Thus, by standard derivation, a general form of effective coupling constants between the scalar quarkonium and pseudoscalar pair is obtained, as shown in Table I.

D. The analyticity of S matrix

By definition, a resonance is specified as a pole of the S matrix analytically continued to the complex s plane. Extracting the poles of the partial-wave amplitude of $i \to j$ process described in the UQM is actually to find the zeros of the determinant of the inverse propagator. Sometimes, it can be obtained in some other equivalent way. For example, in a two-channel occasion the analytically continued S matrices on different Riemann sheets could be written down using those on the first sheet [19]:

$$S^{II} = \begin{pmatrix} \frac{1}{S_{11}} & \frac{iS_{12}}{S_{11}} \\ \frac{iS_{12}}{S_{11}} & \frac{\det S}{S_{11}} \end{pmatrix},$$
$$S^{III} = \begin{pmatrix} \frac{S_{22}}{\det S} & \frac{-S_{12}}{\det S} \\ \frac{-S_{12}}{\det S} & \frac{S_{11}}{\det S} \end{pmatrix}, \quad (11)$$
$$S^{IV} = \begin{pmatrix} \frac{\det S}{S_{22}} & -\frac{iS_{12}}{S_{22}} \\ -\frac{iS_{12}}{S_{22}} & \frac{1}{S_{22}} \end{pmatrix},$$

which implies that a pole on the second Riemann sheet is just located at a zero point of S_{11} on the first sheet, a third-sheet pole at a zero point of $\det S$, and a fourth-sheet pole at a zero of S_{22}, respectively.

In the literature it is common to define a Breit-Wigner mass of a resonance as the solution of $m_{BW}^2 = m_B^2 + \mathrm{Re}\Pi(m_{BW}^2)$. This is a good approximation for narrow resonances and is commonly used in experimental analysis. However, if the propagator is strongly dressed by hadron loops where $\mathrm{Im}\Pi(s)$ is large, the mass and width are no longer suitably determined by the Breit-Wigner form, but should only be defined by the pole position of the S matrix, i.e., the solution of $m_B^2 - s_p + \Pi(s_p) = 0$ with $s_p = (M - i\Gamma/2)^2$. Because of the analyticity of the S matrix, the determinant of inverse propagator vanishes only on unphysical Riemann sheets.

The general character of the poles on different Riemann sheets has been discussed widely in the literature (see, for example, [20,21]). Every physical cut will double the Riemann sheets in the analytical continuation, so there are 2^n Riemann sheets in a process with n coupled channels, as shown in Fig. 1. The physical sheet is defined as the sheet where all the c.m. momenta are positive on the physical cuts, denoted as $(+ + + \cdots +)$ signature. In the same fashion, the $(n+1)^{\text{th}}$ sheet ($n \leq N$), attached to the physical sheet between $s_{\text{th},n}$ and $s_{\text{th},n+1}$ along the physical cut, is denoted by $(- \cdots - + + \cdots)$ with the n consecutive "$-$" signs before the other "$+$" signs. A resonance is represented by a pair of conjugate poles on the Riemann sheet, as required by the real analyticity. The microcausality tells us the first Riemann sheet is free of complex-valued poles, and the resonances are represented by those poles on unphysical sheets. The resonance behavior is only significantly influenced by those nearby poles,

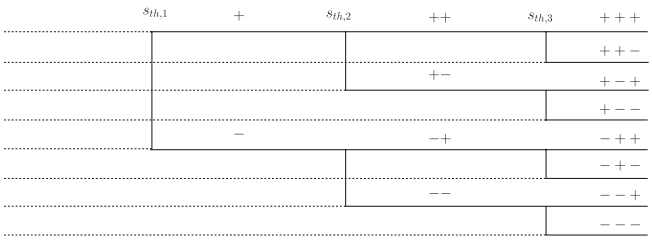

FIG. 1. The right-hand cuts and their signatures in a three-channel case.

and that is why only those closest poles to the experiment region could be extracted from the experiment data in a phenomenological study. Those poles on the other $n > N$ sheets, which are reached indirectly, make less contribution and are thus harder to determine.

III. NUMERICAL ANALYSIS

Now, we apply the partial-wave formulation [2] with our new ingredients to study $I = 1/2$ $K\pi$, $I = 0$ $\pi\pi$, and $I = 1$ $\pi\eta$ S-wave scattering. The main purpose of this paper is not to make an exhaustive fit, so the only data used in the combined fit are: (1) the $I = 1/2$ S-wave $K\pi$ scattering amplitude [22,23], (2) the phase shift of $I = 0$ S-wave $\pi\pi$ scattering [24], and (3) the phase shift of $\pi\pi \to K\bar{K}$ [25] below 1.5 GeV. The fit quality is good and $\chi^2/\text{d.o.f.} \simeq 0.8$. The central values and the statistical errors of the seven parameters are listed in Table II. The good agreement between our theoretical results and experimental data can be seen in Fig. 2, even though some of these data have not been used in the fit. The parameter values in Table II are all in realistic ranges. The bare masses of $q\bar{q}$ states are slightly larger, but not in conflict with NJL modelings [10]. The $SU(3)$ breaking effect parameter is also consistent with the value in the literature [18]. A general comparison of the masses and widths of the resonances from our results and the values from the PDG table is presented in Fig. 3 which will be discussed in detail.

The $I = 1/2$ $K\pi$ S-wave scattering provides an ideal illustration and the best testing ground because of its large threshold spans and clean experimental information. With the parameters of Table II, there is only one solution to $s = (m_0 + m_s)^2 + \text{Re}\Pi(s)$ for real s at about $s^{1/2} = 1.33$ GeV, which is the Breit-Wigner-like mass mentioned previously. However, there are three poles of the S matrix found near the physical region at

$$\begin{aligned}\sqrt{s^{II}} &= 0.767_{\pm 0.009} - i0.308_{\pm 0.035},\\ \sqrt{s^{III}} &= 1.456_{\pm 0.018} - i0.164_{\pm 0.026},\\ \sqrt{s^{IV}} &= 1.890_{\pm 0.029} - i0.296_{\pm 0.014},\end{aligned} \tag{12}$$

where the superscript denotes the number of the sheet and the units are in GeV. Simply comparing these poles with the tables of Particle Data Group [1], a good agreement in quality is instantly found (see Fig. 3). The lowest second-sheet pole is just the κ resonance and consistent with the values determined by those model-independent methods [27]. The third-sheet pole corresponds to the $K_0^*(1430)$ and a second-sheet "shadow" pole (due to the weak coupling constant of the $K\eta$ channel in our result and also found in [21]) is also found at almost the same location. Although the fit is only carried out with the data below 1.5 GeV, a fourth-sheet pole is predicted by the $SU(3)$ couplings and unitarity constraints, which corresponds to the higher $K_0^*(1950)$ resonance. The width of $K_0^*(1950)$ is larger than its PDG value, but is qualitatively acceptable compared with the average value calculated from both solutions A and B of the original data analysis [22,28].

The poles in $I = 0$ $\pi\pi$ S wave are inevitably more complicated than those in the $K\pi$ S wave because of the mixing of $n\bar{n}$ and $s\bar{s}$ states. We find

$$\begin{aligned}\sqrt{s^{II}} &= 0.430_{\pm 0.040} - i0.249_{\pm 0.075},\\ \sqrt{s^{II}} &= 0.986_{\pm 0.015} - i0.023_{\pm 0.022},\\ \sqrt{s^{IV}} &= 1.467_{\pm 0.035} - i0.228_{\pm 0.064},\\ \sqrt{s^{V}} &= 1.577_{\pm 0.040} - i0.306_{\pm 0.023},\\ \sqrt{s^{VI}} &= 1.935_{\pm 0.028} - i0.289_{\pm 0.013},\\ \sqrt{s^{VI}} &= 2.444_{\pm 0.032} - i0.242_{\pm 0.013}.\end{aligned} \tag{13}$$

All these poles could be assigned to those light resonances of $I^G(J^{PC}) = 0^+(0^{++})$ listed in the PDG table, except for the $f_0(1710)$. The position of the σ pole is in agreement with the results of model-independent analysis [29], while the $f_0(980)$ is a narrow pole below the $K\bar{K}$ threshold. The $f_0(1370)$ is a fourth-sheet pole and its position is within the uncertainty of the PDG value. The pole mass is consistent with that preferred by the Belle Collaboration from $\gamma\gamma \to \pi^0\pi^0$, at 1.47 GeV [30]. Here, the resonance shape of $f_0(1500)$ is generated by the fifth-sheet pole and $\eta\eta'$ threshold together, as found in Ref. [31]. This may be the reason why the width of the pole is much wider than the PDG value. The 4π and $\rho\rho$ thresholds turn out to be increasingly important beyond about 1.2 GeV. However, the inclusion of such thresholds requires the SVV and VPP interactions to be taken into account. This would introduce many new parameters and this case is beyond the scope of this paper. Not incorporating the SVV interaction might explain why there is no $f_0(1710)$ pole in this picture. The other possibility is that the main ingredient of $f_0(1710)$ could be the lowest scalar glueball, as preferred by recent quenched lattice calculations [32]. This would add a narrow resonance structure with its own hadron cloud [33]. The two sixth-sheet poles are assigned to the $f_0(2020)$ and the $f_0(2330)$, respectively.

TABLE II. The results of the fit parameters with a Gaussian form factor. m_0, $m_0 + m_s$, and $m_0 + 2m_s$ are the bare masses of $n\bar{n}$, $n\bar{s}$, and $s\bar{s}$ respectively.

α:β:γ	$1.493_{\pm 0.051}$:$(-0.149_{\pm 0.025})$:$0.319_{\pm 0.021}$
ρ	$0.704_{\pm 0.054}$
k_0(GeV)	$0.505_{\pm 0.009}$
m_0(GeV)	$1.443_{\pm 0.020}$
m_s(GeV)	$0.046_{\pm 0.012}$

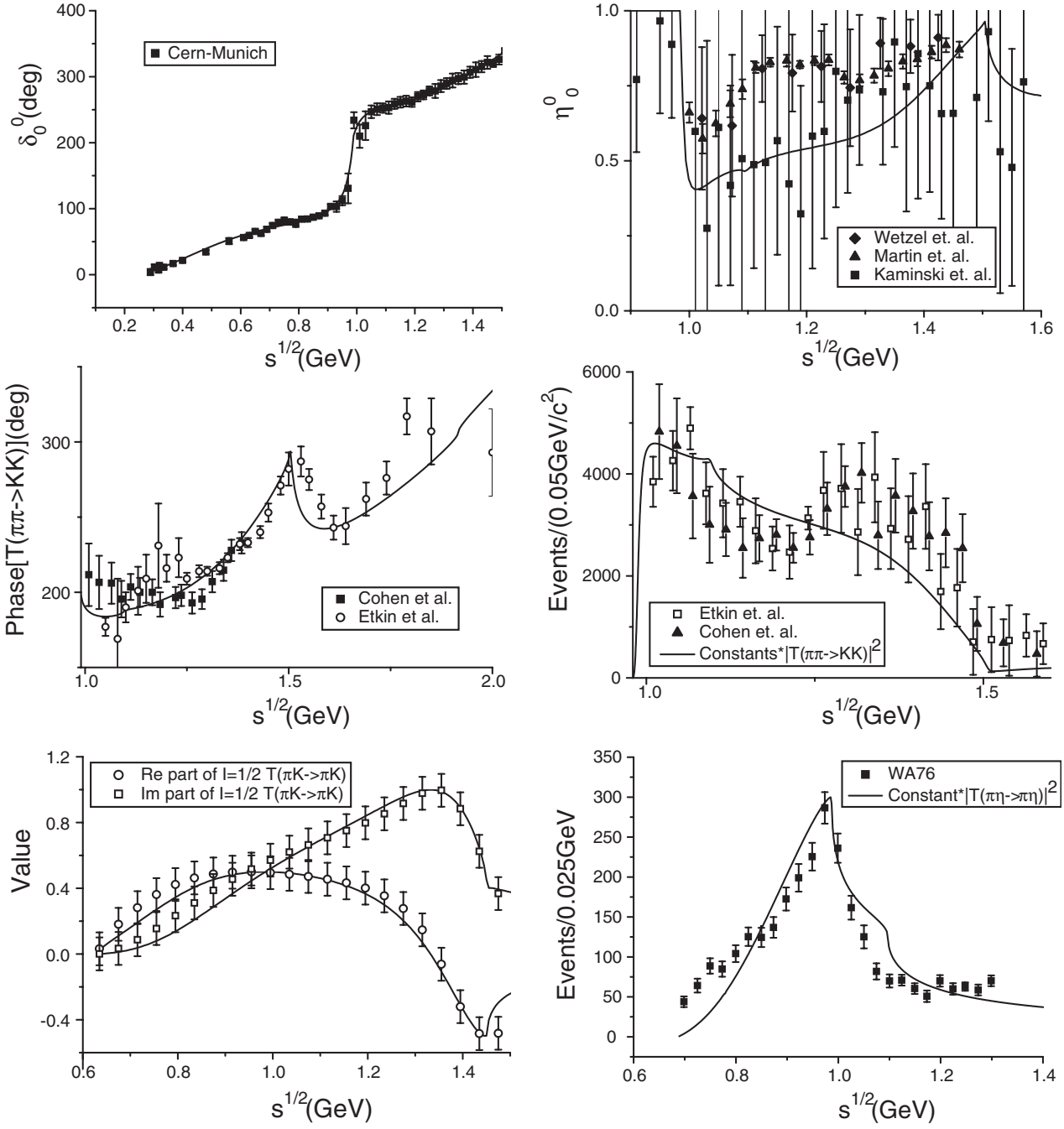

FIG. 2. The left three figures show the fit quality. The right three ones are predictions. Compared data are from [25,26].

As for the $I = 1$ $\pi\eta$ scattering, owing to the poorness of data, this channel is not included in the fit and so the plot in the lower right corner of Fig. 1 is wholly a prediction. As we have mentioned previously, no real-value Adler zero is found up to $O(p^4)$ ChPT amplitude in this partial wave. We simply set $z_A = 0.078$ GeV^2 in the calculation, which is close to the complex zeros. It is not difficult to exhibit the $a_0(980)$ line shape below the $K\bar{K}$ threshold, as shown in Fig. 2. The pole positions are not sensitive to small deviations from the value of Adler zero we choose:

$$\begin{aligned}\sqrt{s^{II}} &= 0.792_{\pm 0.015} - i0.292_{\pm 0.060},\\ \sqrt{s^{III}} &= 1.491_{\pm 0.034} - i0.133_{\pm 0.038},\\ \sqrt{s^{IV}} &= 1.831_{\pm 0.027} - i0.265_{\pm 0.014}.\end{aligned} \tag{14}$$

The second-sheet pole below the $K\bar{K}$ threshold is broad, but still produces the $a_0(980)$ line shape combined with the threshold effect, as proposed by Flatté [34]. This effect was also found by studying the $\pi\eta$ amplitude in the Jülich model [35] and implied in the unitarized σ model [7].

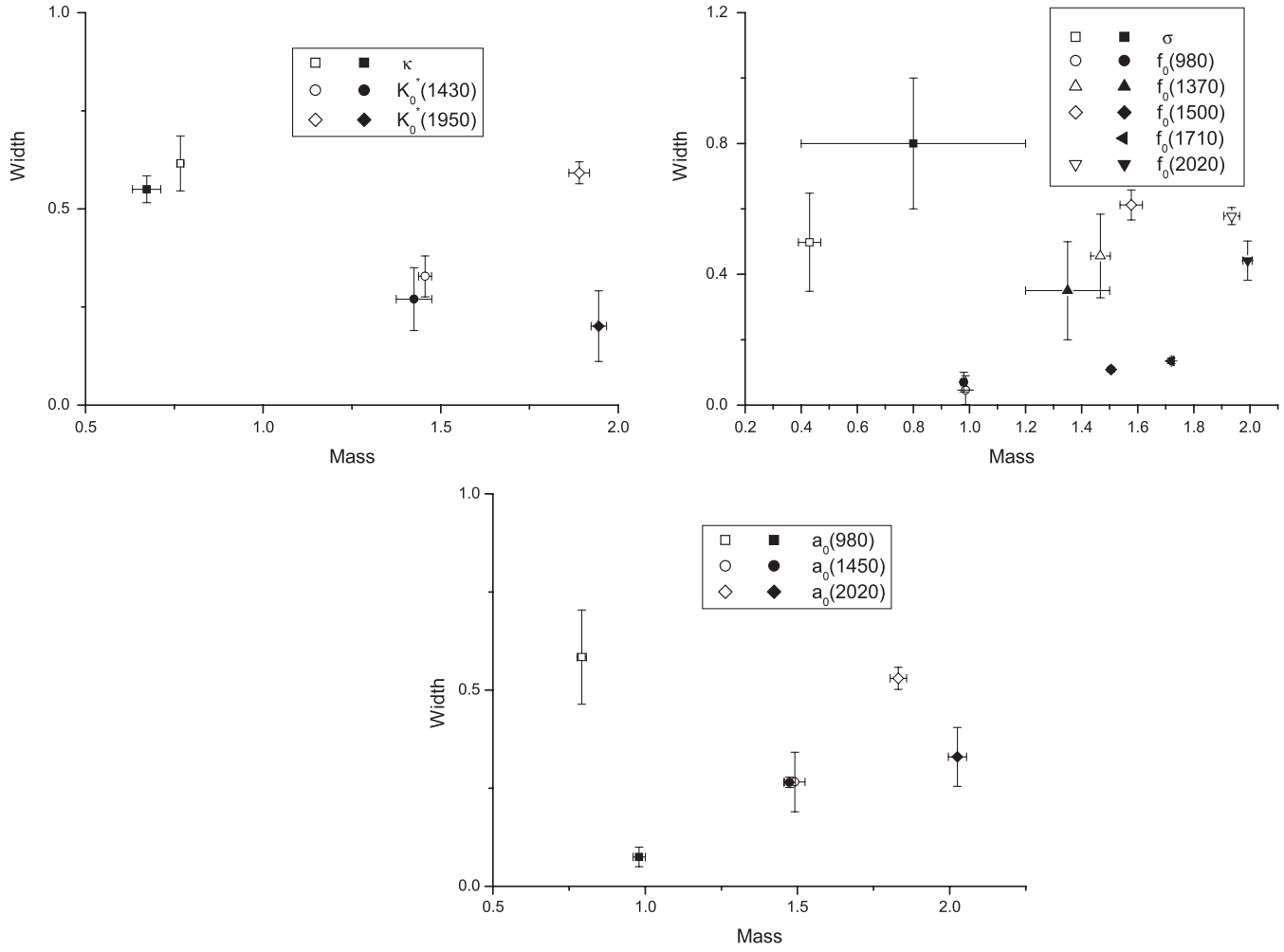

FIG. 3. The filled symbols represent the resonances' masses and widths from the PDG table, and the empty ones represent the pole masses and widths we obtained. The reason of the discrepancy between the value sets has been discussed in the text.

The third-sheet pole could represent the $a_0(1450)$, although it plays a minor role in our picture. There is also a higher $a_0(1830)$ predicted, which has not been widely observed in experiments, but might be related to the $a_0(2020)$ seen by the Crystal Barrel Collaboration [36].

The use of a Gaussian form factor is the most drastic assumption we have made. This has been widely used in experimental analyses and in many other models. However, an exact representation of the form factor, satisfying unitarity and analyticity and easily applied in phenomenological studies, has not been found. To test the stability of our results, we also use a different form factor, $[(M^2 + s_{\mathrm{th},i})/(M^2 + s)]^2$ (M is the mass of the resonance) proposed in [37]. The latter form factor is not better than the Gaussian form factor since it suffers from a spacelike pole, but it might provide a reasonable qualitative cross-check, especially for the N_c analysis we addressed later. Incorporating the latter form factor removes one parameter, k_0, so the fit quality is worse and $\chi^2/\mathrm{d.o.f.} \simeq 1.21$. The central values of the other six parameters listed in Table III are different from those in Table II. Nevertheless, the poles below 1.5 GeV, as shown in the following, coincide in position with those found using the Gaussian form factor:

$$\sqrt{s^{II}} = 0.745_{\pm 0.007} - i0.301_{\pm 0.023},$$
$$\sqrt{s^{III}} = 1.547_{\pm 0.021} - i0.148_{\pm 0.026}, \tag{15}$$

for the $I = 1/2$ channel,

TABLE III. The results of the fit parameters with another form factor.

α:β:γ	$1.889_{\pm 0.024}$:$(-0.280_{\pm 0.015})$:$0.269_{\pm 0.011}$
ρ	$0.821_{\pm 0.027}$
m_0(GeV)	$1.763_{\pm 0.038}$
m_s(GeV)	$0.215_{\pm 0.037}$

$$\sqrt{s^{II}} = 0.396_{\pm 0.019} - i0.244_{\pm 0.046},$$
$$\sqrt{s^{II}} = 0.984_{\pm 0.023} - i0.028_{\pm 0.026}, \quad (16)$$
$$\sqrt{s^{IV}} = 1.455_{\pm 0.037} - i0.304_{\pm 0.040},$$

for the $I = 0$ channel and

$$\sqrt{s^{II}} = 0.700_{\pm 0.060} - i0.265_{\pm 0.031}, \quad (17)$$

for the $I = 1$ channel. The corresponding poles beyond 1.5 GeV still exist, but since we only fit the data below 1.5 GeV and have not included the $I = 1$ data, they move farther away from the previous values. *A posteriori*, this means the second kind of form factor may not be a good choice.

IV. LARGE N_c ANALYSIS OF THE POLE TRAJECTORIES

The success of describing such a broad range of spectrum and their decays in a unified and consistent way suggests that it is a reasonable model to study these resonances and could be used to gain further insights into their nature. The large N_c behavior of the pole trajectories serves to shed light on the origin of these resonances. The lowest order of α is $1/\sqrt{N_c}$, β, and γ by a factor of $1/N_c$ and $1/N_c^2$. The bare mass, the location of Adler zero, and the form factor are of order 1, while the mixing angle ϕ is of order $1/N_c$ [38]. Whichever of our two form factors we use, the poles exhibit similar trajectories as N_c increases. Those for the $I = 1/2, 0$ resonances are shown in Fig. 4 as examples. The σ, κ, and $a_0(980)$ poles move farther away from the real axis. In contrast, the $K_0^*(1430)$ and $K_0^*(1950)$ become narrower and move towards the $n\bar{s}$ bound state. Analogously, the $a_0(1450)$ and $a_0(1830)$ move to the $(u\bar{u} - d\bar{d})/\sqrt{2}$ bare seeds. The f_0 poles other than σ and $f_0(980)$ move towards either the $n\bar{n}$ or $s\bar{s}$ bare seeds. At $N_c = 3$, if the coupling to the $\pi\pi$ channel is switched off, the $f_0(980)$ will move down below the $K\bar{K}$ threshold and form a bound state. This behavior implies that the $f_0(980)$ is more like a $K\bar{K}$ molecule state. However, when N_c increases, it exhibits a peculiar trajectory: it moves to the real axis rapidly and then crosses the cut onto the $(+ - + + +)$ sheet, and then moves away from the real axis as the σ pole does, as seen in Fig. 4. If the coupling to the lowest thresholds are increased, respectively, by hand when $N_c = 3$, the σ, κ, and $a_0(980)$ will move to the real axis and become virtual bound states different from the seeds either. While the coupling becomes strong enough, the virtual bound states will move onto the first sheet and become bound states. It is worth mentioning that, in using the IAM to unitarize ChPT [39], Peláez has observed similar pole behaviors of σ and κ in some parameter region. Using the Padé technique to unitarize ChPT amplitudes, the similar σ pole trajectory is also found [40]. The pole behaviors of $f_0(980)$ and $a_0(980)$, as we pointed out here for the first time, may explain the strange behavior of the line shape in large N_c shown in [39].

So, the general N_c behavior separates the poles into two types: σ, κ, $a_0(980)$, and $f_0(980)$ are the first type (or the unconventional type) of resonances, like bound states of mesons, which are dynamically generated by the pseudoscalar interactions. This may be the reason why they could be described by the tetraquark model. All the other resonances except the glueball candidate, as the second type (or the conventional type) of resonances, are directly generated from $q\bar{q}$ seeds by renormalization effect, which indicates that they all belong to the same bare $q\bar{q}$ nonet. As the interactions are turned on and different channels are open, the bare seeds are copied to different Riemann sheets and get renormalized by the hadron clouds in various ways [21]. Some of them run too far away from the physical

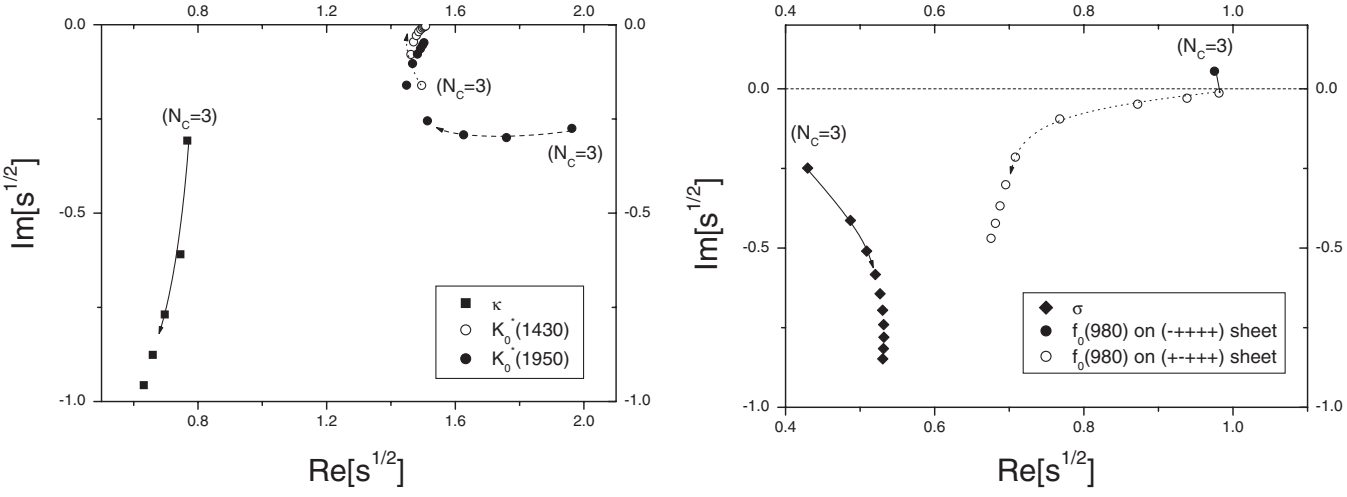

FIG. 4. Left: $I = 1/2$ poles' trajectories; Right: the pole trajectories of σ and $f_0(980)$.

region to be detectable. In this picture, there is no need to distinguish parts of them to be a nonet.

V. SUMMARY

In conclusion, this paper demonstrates that the whole low-energy scalar spectrum below 2.0 GeV, except for a possible glueball $f_0(1710)$, could be described in one consistent picture, with the bare "$q\bar{q}$ seeds" dressed by the hadron loops. All the resonances are dynamically generated by the same mechanism, and there is no direct correspondence between the poles and the original nonet in the Lagrangian. In a large N_c analysis of this picture, the pole trajectories exhibit a general behavior which agrees with other models. In particular, the σ, κ, $f_0(980)$, $a_0(980)$ resonances, though running away from the real axis when N_c is larger, are also generated in this model, which means this large N_c behavior does not conflict with the $q\bar{q}$ dressed by the hadron loop picture. They are produced by large hadron loop effects and this may also imply their large four-quark components. Thus, in this paper, we present that the usual speculation in particle physicist community, that the lighter scalars behave like the tetraquark states and the heavier scalars do as the $q\bar{q}$ states, could be actually realized in such a coherent picture of improved UQM model.

We also show how the line shape of $a_0(980)$ is possibly generated by a deep pole, like the σ or κ, encountering the $K\bar{K}$ threshold. This whole treatment could be extended to other spectra, e.g., the charmonium states [41], and provide theoretical suggestions for further experimental investigation.

ACKNOWLEDGMENTS

We are grateful to Mike Pennington and Hanqing Zheng for instructive discussions and thank Yanrui Liu for helpful discussion. Z. X. thanks the Science and Technology Facilities Council in the United Kingdom for financial support. This work is partly supported by China Scholarship Council and China National Natural Science Foundation under Contracts No. 10705009, No. 10647113, and No. 10875001.

[1] C. Amsler *et al.* (Particle Data Group), Phys. Lett. B **667**, 1 (2008).
[2] N. A. Tornqvist, Z. Phys. C **68**, 647 (1995); N. A. Tornqvist and M. Roos, Phys. Rev. Lett. **76**, 1575 (1996); P. Geiger and N. Isgur, Phys. Rev. D **47**, 5050 (1993); M. Boglione and M. R. Pennington, *ibid.* **65**, 114010 (2002).
[3] E. van Beveren *et al.*, Z. Phys. C **30**, 615 (1986).
[4] R. L. Jaffe, Phys. Rev. D **15**, 267 (1977); L. Maiani *et al.*, Phys. Rev. Lett. **93**, 212002 (2004); G. 't Hooft *et al.*, Phys. Lett. B **662**, 424 (2008).
[5] A. H. Fariborz, R. Jora, and J. Schechter, Phys. Rev. D **77**, 094004 (2008).
[6] D. Lohse *et al.*, Nucl. Phys. **A516**, 513 (1990).
[7] D. Black *et al.*, Phys. Rev. D **64**, 014031 (2001).
[8] P. Minkowski and W. Ochs, Eur. Phys. J. C **9**, 283 (1999).
[9] J. A. Oller, E. Oset, and J. R. Pelaez, Phys. Rev. D **59**, 074001 (1999).
[10] M. X. Su, L. Y. Xiao, and H. Q. Zheng, Nucl. Phys. **A792**, 288 (2007).
[11] M. G. Alford and R. L. Jaffe, Nucl. Phys. **B578**, 367 (2000).
[12] S. L. Adler, Phys. Rev. **139**, B1638 (1965).
[13] V. Weisskopf and E. P. Wigner, Z. Phys. **63**, 54 (1930).
[14] J. Gasser and H. Leutwyler, Ann. Phys. (N.Y.) **158**, 142 (1984).
[15] J. Bijnens, G. Colangelo, G. Ecker, J. Gasser, and M. E. Sainio, Phys. Lett. B **374**, 210 (1996).
[16] V. Bernard, N. Kaiser, and U.-G. Meissner, Phys. Rev. D **44**, 3698 (1991).
[17] J. Gasser and H. Leutwyler, Nucl. Phys. **B250**, 465 (1985).
[18] C. Amsler and F. E. Close, Phys. Rev. D **53**, 295 (1996).
[19] Z. Xiao and H.-Q. Zheng, Commun. Theor. Phys. **48**, 685 (2007).
[20] R. G. Newton, J. Math. Phys. (N.Y.) **2**, 188 (1961).
[21] R. J. Eden and J. R. Taylor, Phys. Rev. **133**, B1575 (1964).
[22] D. Aston *et al.*, Nucl. Phys. **B296**, 493 (1988).
[23] J. M. Link *et al.* (FOCUS Collaboration), Phys. Lett. B **653**, 1 (2007).
[24] W. Ochs, Ph.D. thesis, Munich University, 1974; G. Grayer *et al.*, Nucl. Phys. **B75**, 189 (1974).
[25] D. H. Cohen *et al.*, Phys. Rev. D **22**, 2595 (1980); A. Etkin *et al.*, *ibid.* **25**, 1786 (1982).
[26] W. Wetzel *et al.*, Nucl. Phys. **B115**, 208 (1976); A. D. Martin and E. N. Ozmutlu, *ibid.* **B158**, 520 (1979); R. Kaminski, L. Lesniak, and K. Rybicki, Z. Phys. C **74**, 79 (1997); T. A. Armstrong *et al.* (WA76 Collaboration), *ibid.* **52**, 389 (1991).
[27] H. Q. Zheng *et al.*, Nucl. Phys. **A733**, 235 (2004); Z. Y. Zhou and H. Q. Zheng, *ibid.* **A775**, 212 (2006); S. Descotes-Genon and B. Moussallam, Eur. Phys. J. C **48**, 553 (2006).
[28] A. V. Anisovich and A. V. Sarantsev, Phys. Lett. B **413**, 137 (1997); M. Jamin, J. A. Oller, and A. Pich, Nucl. Phys. **B587**, 331 (2000).
[29] Z. Y. Zhou *et al.*, J. High Energy Phys. 02 (2005) 043; I. Caprini, G. Colangelo, and H. Leutwyler, Phys. Rev. Lett. **96**, 132001 (2006).
[30] S. Uehara *et al.* (Belle Collaboration), Phys. Rev. D **78**, 052004 (2008).
[31] M. Albaladejo and J. A. Oller, Phys. Rev. Lett. **101**, 252002 (2008).

[32] W.-J. Lee and D. Weingarten, Phys. Rev. D **61**, 014015 (1999); C. Liu, Chin. Phys. Lett. **18**, 187 (2001); Y. Chen *et al.*, Phys. Rev. D **73**, 014516 (2006).
[33] M. Boglione and M. R. Pennington, Phys. Rev. Lett. **79**, 1998 (1997).
[34] S. M. Flatte, Phys. Lett. **63B**, 224 (1976).
[35] G. Janssen *et al.*, Phys. Rev. D **52**, 2690 (1995).
[36] A. V. Anisovich *et al.* (Crystal Barrel Collaboration), Phys. Lett. B **452**, 173 (1999).
[37] F. Ravndal, Phys. Rev. D **4**, 1466 (1971).
[38] G. 't Hooft, Nucl. Phys. **B72**, 461 (1974); E. Witten, *ibid.* **B160**, 57 (1979).
[39] J. R. Pelaez, Phys. Rev. Lett. **92**, 102001 (2004).
[40] Z. X. Sun, L. Y. Xiao, Z. Xiao, and H. Q. Zheng, Mod. Phys. Lett. A **22**, 711 (2007).
[41] M. R. Pennington and D. J. Wilson, Phys. Rev. D **76**, 077502 (2007).